

PSFC/JA-11-33

Lower hybrid current drive at high density in the multi-pass regime

G.M. Wallace¹, I.C. Faust¹, O. Meneghini¹, R.R. Parker¹, S. Shiraiwa¹, S.G. Baek¹, P.T. Bonoli¹, A.E. Hubbard¹, J.W. Hughes¹, B.L. LaBombard¹, C. Lau¹, Y. Ma¹, M.L. Reinke¹, A.E. Schmidt^{1*}, J.L. Terry¹, D.G. Whyte¹, J.C. Wright¹, and S.J. Wukitch¹, R.W. Harvey², A.P. Smirnov³, J.R. Wilson⁴

¹MIT Plasma Science and Fusion Center, Cambridge, MA 02139

²CompX, Del Mar, CA 92014

³M.V. Lomonosov Moscow State University, Moscow, Russia

⁴Princeton Plasma Physics Laboratory, Princeton, NJ 08543

*Present affiliation: Lawrence Livermore National Laboratory, Livermore, CA 94550

December, 2011

**Plasma Science and Fusion Center
Massachusetts Institute of Technology
Cambridge MA 02139 USA**

This work was supported by the U.S. Department of Energy, Grant No. DE-FC02-99ER54512 and DE-AC02-09CH11466. Reproduction, translation, publication, use and disposal, in whole or in part, by or for the United States government is permitted.

Lower hybrid current drive at high density in the multi-pass regime

G.M. Wallace, I.C. Faust, O. Meneghini, R.R. Parker, S. Shiraiwa, S.G. Baek, P.T. Bonoli, A.E. Hubbard, J.W. Hughes, B.L. LaBombard, C. Lau, Y. Ma, M.L. Reinke, J.L. Terry, D.G. Whyte, J.C. Wright, and S.J. Wukitch
MIT Plasma Science and Fusion Center, Cambridge, MA 02139

R.W. Harvey
CompX, Del Mar, CA 92014

A.E. Schmidt
*MIT Plasma Science and Fusion Center, Cambridge,
MA 02139 Present affiliation: Lawrence Livermore
National Laboratory, Livermore, CA 94550*

A.P. Smirnov
M.V. Lomonosov Moscow State University, Moscow, Russia

J.R. Wilson
Princeton Plasma Physics Laboratory, Princeton, NJ 08543

(Dated: December 12, 2011)

Abstract

Assessing the performance of lower hybrid current drive (LHCD) at high density is critical for developing non-inductive current drive systems on future steady-state experiments. Excellent LHCD efficiency has been observed during fully non-inductive operation ($\eta = 2.0 - 2.5 \times 10^{19}$ AW⁻¹m⁻² at $\bar{n}_e = 0.5 \times 10^{20}$ m⁻³) on Alcator C-Mod [I. H. Hutchinson, *et al*, Physics of Plasmas, **1**, 1511 (1994)] under conditions (n_e , magnetic field and topology, LHCD frequency) relevant to ITER [S. Shiraiwa, *et al*, Nuclear Fusion, **51**, 103024 (2011)]. To extend these results to advanced tokamak regimes with higher bootstrap current fractions on C-Mod, it is necessary to increase \bar{n}_e to $1.0 - 1.5 \times 10^{20}$ m⁻³. However, the number of current-carrying, non-thermal electrons generated by LHCD drops sharply in diverted configurations at densities that are well below the density limit previously observed on limited tokamaks. In these cases, changes in scrape off layer (SOL) ionization and density profiles are observed during LHCD, indicating that significant power is transferred from the LH waves to the SOL. Fokker-Planck simulations of these discharges utilizing ray tracing and full wave propagation codes indicate that LH waves in the high density, multi-pass absorption regime linger in the plasma edge and SOL region, where absorption near or outside the LCFS results in the loss of current drive efficiency. Modeling predicts that non-thermal emission increases with stronger single-pass absorption. Experimental data show that increasing T_e in high density LH discharges results in higher non-thermal electron emission, as predicted by the models.

PACS numbers: 52.35.Hr, 52.50.Sw, 52.65.Ff, 52.55.Wq

I. INTRODUCTION

The Lower Hybrid Current Drive (LHCD) system [1] on Alcator C-Mod [2] is designed to investigate advanced, non-inductive operation [3] with plasma conditions relevant to future devices such as ITER [4]. Experiments on C-Mod have shown that the critical density associated with reduced current drive occurs at a value significantly lower than what would have been expected based on prior LHCD experiments [5, 6]. These results suggest that interactions between LH waves and the SOL plasma have a substantial impact on the operational effectiveness of a LHCD system in high density diverted discharges.

Lower hybrid current drive [7, 8] has proven to be an efficient mechanism for non-inductive operation and current profile control [9] on the Alcator C-Mod tokamak at low to moderate densities ($\bar{n}_e = 0.4 - 0.8 \times 10^{20} \text{ m}^{-3}$). The second generation (“LH2”) LHCD antenna on Alcator C-Mod [10] consists of a slow wave launching structure located on the low field side mid-plane. The launcher has 64 waveguides arranged in 16 columns and 4 rows. Power is distributed from a single feed waveguide to the four launching waveguides in each column by a novel 4-way splitter system [11]. The LHCD system is powered by ten 250 kW klystrons operating at 4.6 GHz for a nominal source power of 2.5 MW. The launched wavenumber spectrum is controlled by adjusting the relative phasing between waveguides in the array [12]. The resulting wavenumber spectrum is asymmetric in the toroidal direction, with most of the power launched in the electron current direction, and about 20% of the power in the opposite direction. The peak of the main $n_{||} \equiv ck_{||}/\omega$ lobe on C-Mod can be adjusted from 1.5-3.

LH waves drive current by transferring momentum and energy from the wave to electrons traveling along the magnetic field through Landau damping. The phase velocity of the wave, $v_{||} = c/n_{||}$, must be approximately $3v_{te}$ for strong electron Landau damping to occur on a Maxwellian electron distribution. Here the electron thermal speed is defined as $v_{te} = \sqrt{2T_e/m_e}$. Once a non-thermal electron tail is formed, the waves can damp quasi-linearly at higher phase velocities. This results in an asymmetric distribution function where electrons at high parallel velocity ($v_{||}/c \sim 0.5$) carry most of the non-inductive current, resulting in a high current drive efficiency ($J/P \propto 1/(n_e n_{||}^2)$) [7, 8].

Figure 1 shows a typical non-inductive discharge on Alcator C-Mod. The loop voltage is reduced to zero within the error produced by the feedback controller for several current

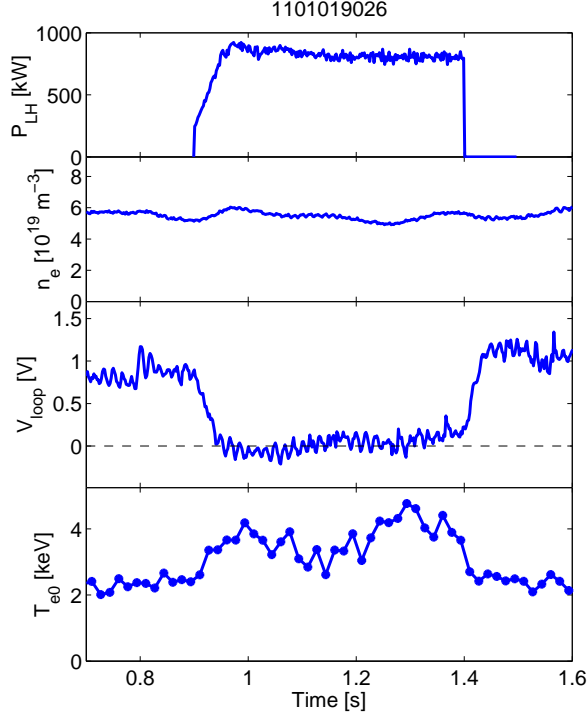


FIG. 1: (Color on-line) Plasma parameters during a typical non-inductive discharged with LHCD on Alcator C-Mod. From top to bottom: LH power, line averaged density, loop voltage, and central electron temperature versus time.

relaxation timescales ($\tau_R \sim 200$ ms) [10]. The central safety factor, q_0 , increases above unity due to the broader current drive profile, which suppresses saw-teeth and causes the core temperature to rise during the non-inductive phase of the discharge. The normalized current drive efficiency, $\eta \equiv n_e I_p R_0 / P_{LH}$, for non-inductive discharges at low density on C-Mod is $2.0 - 2.5 \times 10^{20} \text{ AW}^{-1} \text{ m}^{-2}$. Lower hybrid current drive provides nearly all of the current drive since the bootstrap current is negligible in these low density L-mode discharges.

Reactor relevant advanced scenarios on C-Mod require that the self-generated bootstrap current be a significant fraction of the total plasma current. These advanced scenarios benefit from higher plasma densities ($\bar{n}_e = 1.1 - 1.5 \times 10^{20} \text{ m}^{-3}$) than the non-inductive discharges discussed above. TRANSP [13] simulations predict an attractive regime with roughly equal bootstrap and LH current fractions ($f_{BS} \sim f_{LHCD} \sim 50\%$) on C-Mod at $\bar{n}_e \sim 1.3 \times 10^{20} \text{ m}^{-3}$ [14]. It should be noted that the LSC [15] package used to calculate the LH driven current

in TRANSP assumes that all launched LH wave power will be absorbed inside the LCFS. This assumption results in a normalized current drive efficiency, η , that is nearly constant as a function of density. It is of critical importance to determine the validity of this assumption at higher density when planning future advanced scenario experiments.

The maximum density at which efficient LHCD is observed on limited tokamaks is set by the conditions for wave accessibility [16, 17] and parametric decay instabilities [18, 19]. If one considers only the accessibility criterion, then any wave for which n_{\parallel} is locally greater than $n_{\parallel,crit}$ everywhere in the plasma will be able to penetrate to the core of the plasma, provided that the wave is not absorbed at a larger minor radius. Here,

$$n_{\parallel,crit} \approx \sqrt{1 - \frac{\omega_{pi}^2}{\omega_0^2} + \frac{\omega_{pe}^2}{\omega_{ce}^2} + \frac{\omega_{pe}}{|\omega_{ce}|}}, \quad (1)$$

where ω_{pi} is the ion plasma frequency, ω_{pe} is the electron plasma frequency, ω_{ce} is the electron cyclotron frequency, and ω_0 is the launched LH wave frequency. Penetration of the waves to the plasma core is also limited by refraction. As the waves propagate into regions of higher electron density, the angle between the group velocity and the magnetic field is reduced until the group velocity becomes tangent to the field. At this point, the wave turns and propagates back towards the plasma edge where it will be reflected at the cutoff layer. In the absence of absorption, the waves will continue to reflect and refract, eventually filling the plasma volume.

Parametric decay instabilities [20, 21] are a three wave coupling process by which an incident lower hybrid wave at a frequency $\omega = \omega_0$ decays into a low frequency branch, at $\omega = \omega_1 \sim \omega_{ci} \ll \omega_0$, and a daughter LH wave, at $\omega = \omega_0 - \omega_1$. The wavenumber of the daughter LH wave may increase substantially, thereby reducing the current drive efficiency. If the up-shift of n_{\parallel} is severe enough the daughter wave may damp on ions as well. A threshold for strong parametric decay occurs at $\omega_0/\omega_{LH} \leq 2$. Because ω_{LH} scales with both magnetic field and density, parametric decay is of particular importance on high field, high density experiments such as Alcator C [19].

Bremsstrahlung emission in the 40-200 keV range can be used as a sensitive proxy for the population of fast electrons generated by LHCD. A hard x-ray (HXR) camera is installed on C-Mod to measure the bremsstrahlung emission from these fast electrons [22]. The HXR camera has 32 viewing chords arranged in a poloidal array, with chord 1 viewing the bottom of the plasma and chord 32 viewing the top. Chords 9-24 are used in this paper to determine

the non-thermal electron population in the plasma core (see inset of Figure 2). The use of bremsstrahlung as a diagnostic can become problematic when the noise generated by fusion neutrons exceeds the bremsstrahlung signal level, such as in the case of hot, dense, deuterium discharges, or when there is a significant contribution from thick-target bremsstrahlung from the inner wall, such as in inner wall limited discharges. In these circumstances, the fast electron population is diagnosed using non-thermal electron cyclotron emission (ECE), although the non-thermal ECE is more difficult to interpret quantitatively due to the mixing of spatial and energy information intrinsic to the measurement.

The remaining sections of this paper will describe experimental results of LHCD at high density on Alcator C-Mod and interpretation of these results using ray tracing and full wave modeling. Specifically, the population of fast electrons generated by LHCD falls steeply as a function of density for diverted discharges, but the current drive effect is recovered at high density for inner wall limited and higher temperature diverted discharges. Changes in the SOL density and line emission profiles indicate that significant LH wave power may be absorbed outside the LCFS. Full wave and ray tracing modeling show that power absorption moves very far off-axis at high density and agree qualitatively with the experimental results.

II. EXPERIMENTAL RESULTS

Non-thermal electron bremsstrahlung falls exponentially as a function of line averaged density in diverted discharges without ion cyclotron heating on Alcator C-Mod [6] (green data points in Figure 2). Non-thermal ECE also declines rapidly as density rises, and little or no non-thermal emission is seen at high density ($\bar{n}_e = 1.2-1.5 \times 10^{20} \text{ m}^{-3}$) in these discharges. Additionally, the plasma loop voltage does not decrease in magnitude when LH waves are applied to high density discharges, which confirms that there are few, if any, fast electrons generated by LHCD. This drop in the population of LH driven fast electrons for diverted discharges occurs at a lower density than anticipated based on earlier high density LHCD experiments on limited tokamaks [18, 19], or by conventional ray-tracing/Fokker-Planck modeling (solid line in Figure 2). The exponential drop in non-thermal bremsstrahlung is not associated with a violation of the accessibility criterion defined in the previous section [6]. Furthermore, $\omega/\omega_{LH} \sim 4$, well above the PDI threshold at $\omega/\omega_{LH} = 2$. Simulations using the ray tracing/Fokker-Planck package GENRAY/CQL3D [23, 24] do not predict a

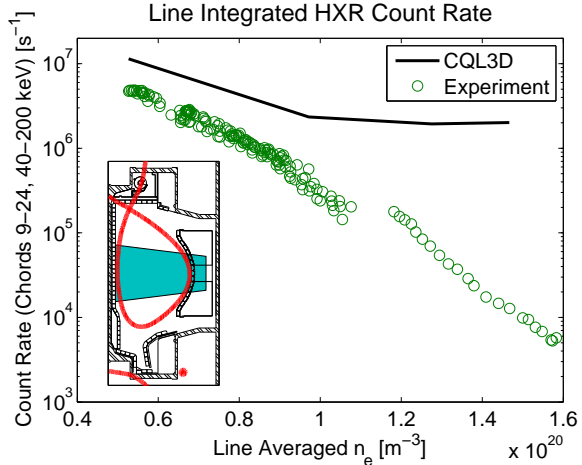


FIG. 2: (Color on-line) Experimental fast electron bremsstrahlung from the core plasma as a function of line averaged density (points) and the synthetic diagnostic prediction from GENRAY/CQL3D when no SOL is included in the model. The shaded region of the inset indicates the viewing geometry of HXR chords 9-24.

sharp decline in non-thermal emission as density increases when SOL losses are not included in the model.

The expected current drive dependence is recovered for limited discharges on C-Mod above 10^{20} m^{-3} [5]. Figure 3 shows core HXR emission as a function of density for inner wall limited (IWL) and diverted discharges. These results agree with current drive experiments at high density ($\bar{n}_e = 1.0 - 1.5 \times 10^{20} \text{ m}^{-3}$) on Alcator C [25, 26]. The IWL discharges exhibit HXR emission 2-3 orders of magnitude higher than diverted discharges at $\bar{n}_e = 1.5 \times 10^{20} \text{ m}^{-3}$, while HXR emission from diverted discharges with small gaps ($< 0.5 \text{ cm}$) between the plasma and the inner wall fall between the IWL discharges and the diverted discharges with large ($> 1.0 \text{ cm}$) inner gaps. Some of the HXR emission from inner wall limited discharges may be due to thick-target bremsstrahlung generated by electrons striking the inner wall, but the increase of the fast electron population in IWL discharges as compared to diverted discharges is confirmed by both the non-thermal ECE and by changes in the plasma loop voltage.

Although line averaged density and edge neutral pressure are closely correlated, the relationship between the two quantities is quite different for limited and diverted discharges. Fueling efficiency is significantly higher in limited discharges, and consequently the edge

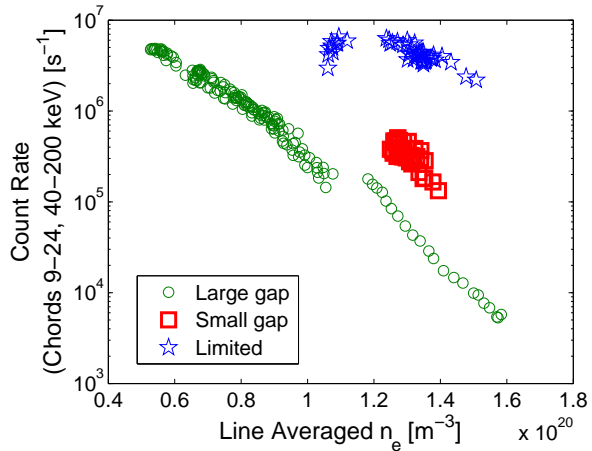


FIG. 3: (Color on-line) Experimental fast electron bremsstrahlung from the core plasma as a function of line averaged density for diverted discharges with large inner gaps (green circles), diverted discharges with small inner gaps (red squares), and inner wall limited discharges (blue stars).

neutral pressure is lower for a limited discharge as compared to a diverted discharge at the same line averaged density. Figure 4 shows the line integrated HXR emission as a function of mid-plane neutral pressure for various plasma configurations. HXR count rates from limited and diverted discharges, which are significantly different when plotted as functions of line averaged density, lie on the same trend line when plotted as functions of neutral pressure.

The response of SOL density profiles to high power LH also differ between limited and diverted discharges. Figure 5 shows the SOL density profile in front of the LH launcher as measured by an X-mode reflectometer [27] for diverted and limited discharges. The limited discharge shows a modest increase in density in the far SOL ($R - R_{LCFS} > 1$ cm) when high power LH waves are applied to the plasma, while the diverted discharge exhibits a more pronounced increase of density in the far SOL during LH. Profiles in the near SOL ($R - R_{LCFS} < 1$ cm) do not change significantly, suggesting that there is a localized source of particles in the far SOL.

Ionization of neutral particles in the SOL appears to be a significant power sink for the LH waves. Figures 6 and 7 show the Abel inverted SOL ionization light profiles for diverted deuterium and helium discharges at moderate to high densities. The total amount of ionization light increases when high power ($P_{LH} > \sim 300$ kW) LH is applied as compared

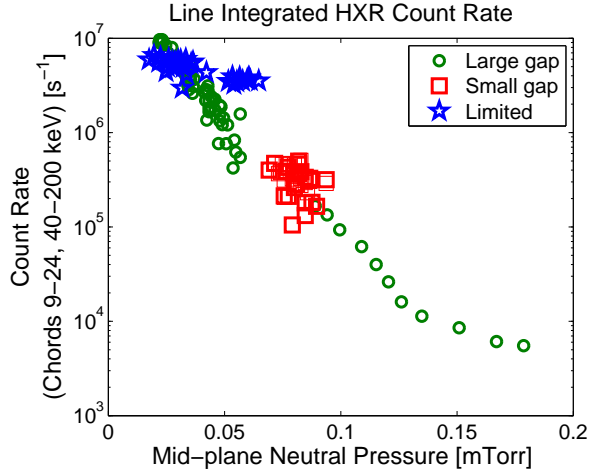


FIG. 4: (Color on-line) Experimental fast electron bremsstrahlung from the core plasma as a function of mid-plane neutral pressure for diverted discharges with large inner gaps (green circles), diverted discharges with small inner gaps (red squares), and inner wall limited discharges (blue stars).

to when there is no LH power. The peak of the ionization light profile also moves farther away from the last closed flux surface (LCFS) when LH is on. The shift in the ionization profile indicates that there is an increase in power dissipated in the far SOL.

The increased ionization during LH extends into the shadow of the main plasma and local LH protection limiters on the low field side (LFS). This ionization cannot be due to absorption of LH waves in the SOL on the first pass from the antenna to the LCFS, but rather from waves which have traveled back into the SOL after passing through the plasma. If the source of additional ionization power were from cross-field transport of LH power absorbed inside the LCFS, one would expect the profiles shown in Figure 5 to change in the near SOL as well as the far SOL. The ionization profiles in Figures 6 and 7 shift outwards, indicating that more power is dissipated in the far SOL. This suggests that the LH waves travel extensively through the SOL, filling the volume bounded by the slow wave cutoff layer (located where $n_e = 2.7 \times 10^{17} \text{ m}^{-3}$ at 4.6 GHz). The increased ionization in the far SOL is also consistent with observations of density increases in the SOL measured with Langmuir probes and the X-mode reflectometer discussed previously. The measurements in Figures 6 and 7 are from toroidal views near the plasma mid-plane on the LFS of the tokamak. Assuming that the ionization is uniformly distributed toroidally and poloidally,

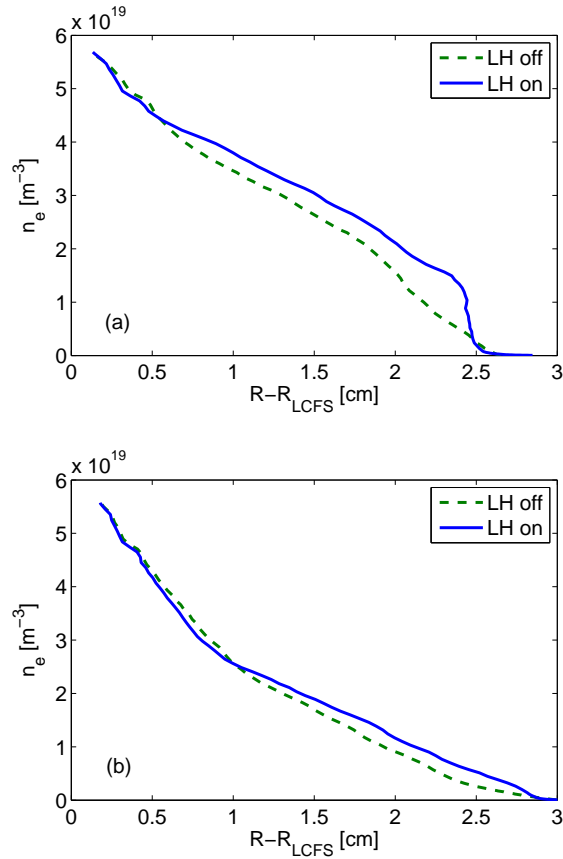


FIG. 5: (Color on-line) Scrape off layer density profiles measured in front of the LH launcher with the X-mode reflectometer system with and without high power (~ 500 kW) LH in diverted (a) and limited (b) discharges.

the increased ionization power in the SOL is in excess of 100 kW.

According to simple theory [8] and model predictions [14], increasing plasma temperature should result in stronger single-pass absorption of the LH waves inside the LCFS. Figure 8 shows that hotter I-mode discharges, which have an L-mode like density profile with an H-mode like temperature profile [28–30], exhibit higher non-thermal ECE than L-modes at the same density.

Experiments with high temperature helium discharges were conducted to examine the effect of increased electron temperature on HXR emission produce by LHCD without contaminating the HXR signal with fusion neutrons [14]. The I-mode regime has not yet been extended to operation with helium as the main ion species, but hot L-mode discharges in

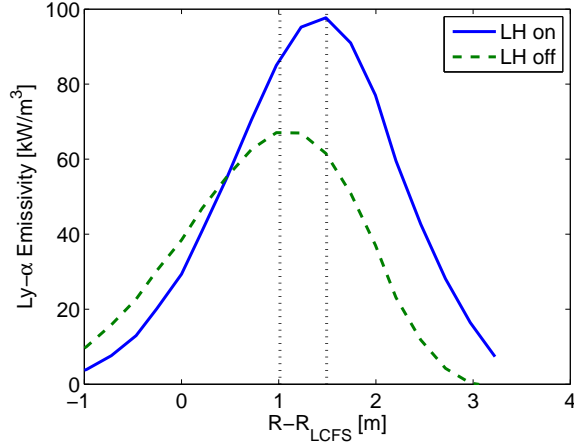


FIG. 6: (Color on-line) Ly- α emissivity profiles with and without high power (~ 700 kW) LH in a diverted deuterium discharge at $\bar{n}_e = 1.1 \times 10^{20} \text{ m}^{-3}$. The vertical dotted lines represent the main limiter position (left) and LH launcher position (right).

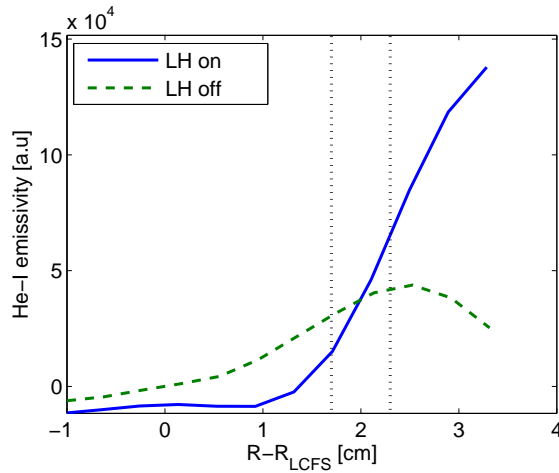


FIG. 7: (Color on-line) He-I emissivity profiles with and without high power (~ 600 kW) LH in a diverted helium discharge at $\bar{n}_e = 1.5 \times 10^{20} \text{ m}^{-3}$. The vertical dotted lines represent the main limiter position (left) and LH launcher position (right).

helium show a significant increase in HXR as compared to cold deuterium discharges at line averaged densities between 1.1×10^{20} and $1.6 \times 10^{20} \text{ m}^{-3}$. This can be seen by comparing the blue/green circles (1-3 keV deuterium discharges) with the orange/red diamonds (3.5-4.5 keV helium discharges) in Figure 9. The mode conversion heating scenario used in these

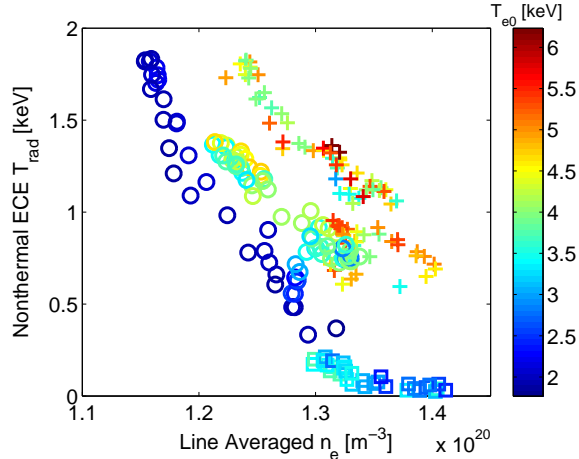


FIG. 8: (Color on-line) Experimental non-thermal ECE as a function of line averaged density for L- (circles, squares) and I-mode (+ symbols) discharges on C-Mod. The color of the data points corresponds to T_{e0} in keV.

discharges required high magnetic field ($B_\phi = 8$ T) to deposit power on axis. The plasma current was also increased to 1.2 MA to improve energy confinement and keep the safety factor similar to the 5.4 T, 0.8 MA deuterium discharges. Increasing plasma current and magnetic field in deuterium results in higher non-thermal emission at high density [6], but the increase in HXR emission in the hot helium discharges is larger than would be expected based on the change in current and magnetic field alone.

III. DISCUSSION

Many of the experimental observations presented in this paper point towards absorption of LH waves near or outside the last closed flux surface as a significant power loss channel for LH waves in high density diverted discharges. A SOL model including LH wave dissipation due to electron-ion collisions [31] has been added to the GENRAY/CQL3D ray-tracing/Fokker-Planck model to examine the impact of the SOL on LHCD at high density [6]. Damping due to electron-ion collisions is calculated by replacing the electron mass with $m_e(1 + i\nu_{ei}/\omega_0)$ in the momentum equations [31], where ν_{ei} is the electron-ion collision frequency. This model predicts that a large fraction of the LH wave power is absorbed by electron-ion collisions outside the LCFS at high density. Figure 10 shows the relative fractions of power absorbed

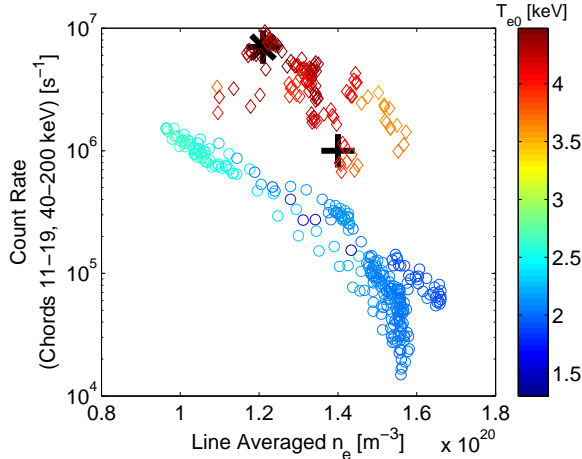


FIG. 9: (Color on-line) Experimental fast electron bremsstrahlung from the core plasma as a function of line averaged density. The color of the data points corresponds to T_{e0} in keV. Circles represent data from 5.4 T, 800 kA deuterium discharges, while diamonds represent data from 8 T, 1.2 MA helium discharges. The large + symbol indicates the HXR emission predicted by GENRAY/CQL3D for a discharge with $T_{e0} = 4$ keV. The large asterisk indicates the HXR emission predicted by LHEAF/VERD for a discharge with $T_{e0} = 4.3$ keV

inside and outside the LCFS as a function of line averaged density. At $\bar{n}_e = 0.5 \times 10^{20} \text{ m}^{-3}$ less than 20% of the forward power is absorbed outside the LCFS, while at $1.5 \times 10^{20} \text{ m}^{-3}$ about 50% of the forward power is absorbed outside the LCFS. Nearly all of the power launched in the counter-current lobe (approximately 20% of the total power) is absorbed on the first pass by electron Landau damping inside the LCFS.

The results shown in Figure 10 assume a minimum SOL temperature, T_{min} , of 5 eV and $Z_{eff} = 1.8$. The amount of power absorbed by electron-ion collisions is quite sensitive to the electron-ion collision frequency, and thus the SOL temperature, density, and Z_{eff} profiles ($\nu_{ei} \propto n_e Z_{eff} T_e^{-1.5}$). A sensitivity scan of the T_{min} and Z_{eff} parameters is shown in Figure 11. The synthetic diagnostic is still higher than the experimental HXR count rate at high density for the $Z_{eff} = 4.0$, $T_{min} = 10$ eV case when viewed on a logarithmic plot (compare the green circles and the dashed/dash-dotted lines in Figure 11), but the amount of HXR emission (and driven current) is very small as compared to the modeling without SOL absorption (solid black line) for both the model with SOL absorption and the experiment.

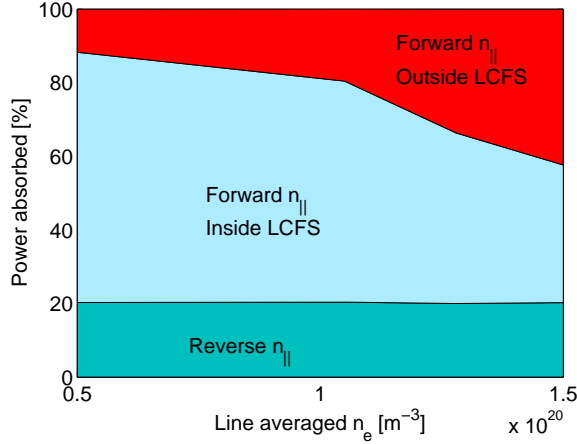


FIG. 10: (Color on-line) Simulated power absorption from GENRAY/CQL3D as a function of line averaged density assuming $Z_{eff} = 1.8$ and $T_{min} = 5$ eV in the SOL.

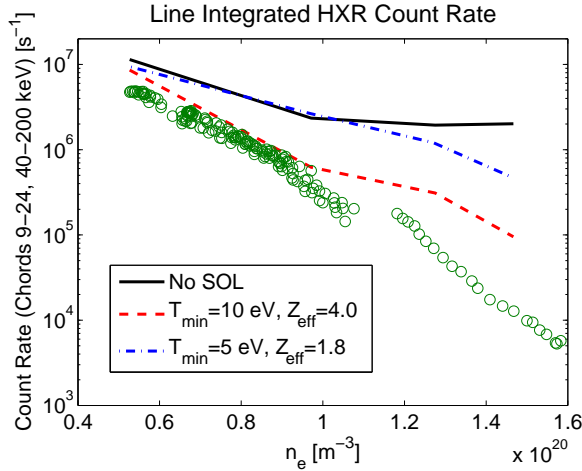


FIG. 11: (Color on-line) Simulated HXR emission from GENRAY/CQL3D as a function of line averaged density assuming $Z_{eff} = 1.8$ and $T_{min} = 5$ eV in the SOL (blue dash-dotted line), $Z_{eff} = 4$ and $T_{min} = 10$ eV in the SOL (red dashed line), and no absorption in the SOL (solid black line). Green circles are experimental HXR count rates.

The simulations shown in Figures 10 and 11 include only the effects of electron-ion collisions. The scaling of HXR emission with neutral pressure (Figure 4) implies that electron-neutral collisions may be another important loss mechanism for LH waves in high density diverted discharges. Two issues must be resolved in order to assess the potential impact of

electron-neutral collisions in the modeling. First it is necessary to determine 2-D profiles of the neutral species to use as inputs for the calculation. These profiles are not yet available for C-Mod discharges, but recent diagnostic upgrades combined with edge modeling tools will make it possible to reconstruct the neutral density profiles in future experiments. Losses due to elastic electron-neutral collisions may be included in the simulations in a manner similar to the treatment of elastic electron-ion collisions discussed above.

The second issue to address is the development of an appropriate model for inelastic electron-neutral collisions and electron impact ionization. Damping of LH waves by ionization is an inherently non-linear process, and considerable effort must be made to extend the model to include this. Ionization cross sections are readily available and future code development will incorporate ionization into the collisional damping calculation. The changes in SOL density and ionization profiles during LH at high density are direct evidence that LH wave power is dissipated by the ionization of neutral particles. Simple estimates of excess power lost due to this ionization (assuming poloidal and toroidal symmetry) indicate that excess ionization power of at least 100 kW is dissipated when LH is on compared to the Ohmic portions of the discharge at high density. Adding the power lost due to ionization to the power damped by electron-ion collisions may account for most of the launched LH power.

Simulations of high density C-Mod discharges with the full wave/Fokker-Planck codes LHEAF/VERD [32] indicate that LH waves are absorbed just inside the LCFS ($0.8 < r/a < 1$) rather than in the SOL [33]. Only 7% of the forward wave power is absorbed by collisional damping outside the LCFS at $\bar{n}_e = 1.3 \times 10^{20} \text{ m}^{-3}$ in the LHEAF/VERD simulation, as compared with about 40% in the GENRAY/CQL3D simulation. GENRAY/CQL3D and LHEAF/VERD predict similar declines in fast electron bremsstrahlung as density increases. The LHEAF/VERD simulation shows that LH waves experience a significant $n_{||}$ upshift when reflecting from the plasma edge [34]. This upshift is strong enough to cause the waves to Landau damp on electrons at $\sim 3v_{te}$ near the edge [35]. The low temperature and high $n_{||}$ in the edge result in a very poor current drive efficiency, and therefore weak bremsstrahlung emission. Figure 12 shows the power deposition profiles calculated by LHEAF/VERD and GENRAY/CQL3D for a high density ($\bar{n}_e = 1.3 \times 10^{20} \text{ m}^{-3}$) diverted L-mode discharge on C-Mod. Both the full wave and ray tracing calculations predict that the power absorption for $r/a < 0.8$ is weak compared with the power absorption in the edge and SOL regions

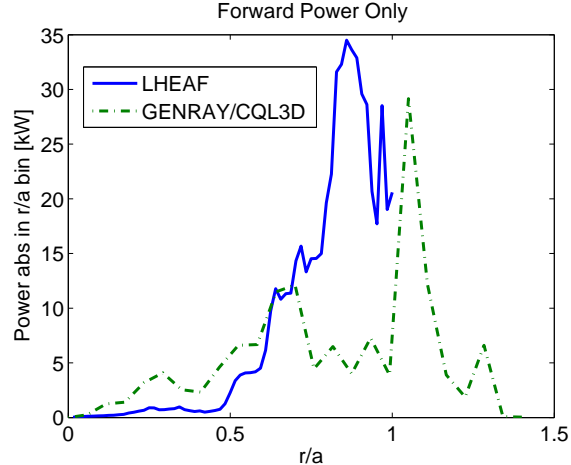


FIG. 12: (Color online) Comparison of power damping profiles calculated by ray tracing (GENRAY/CQL3D) and full wave (LHEAF/VERD) models of a C-Mod discharge at $\bar{n}_e = 1.3 \times 10^{20} \text{ m}^{-3}$. The damping profiles shown are for the forward n_{\parallel} lobe only. The full wave model predicts most of the power to be absorbed just inside the LCFS ($0.8 < r/a < 1.0$) while the ray tracing model predicts significant power absorption just outside the LCFS ($1.0 < r/a < 1.2$).

($r/a > 0.8$). The full wave model predicts most of the power to be absorbed just inside the LCFS ($0.8 < r/a < 1.0$) while the ray tracing model predicts significant power absorption just outside the LCFS ($1.0 < r/a < 1.2$).

The ray tracing and full wave results shown in Figure 12 represent two different simulations of the same discharge and should not be taken as a direct comparison of ray tracing and full wave techniques. The temperature and density profiles used in the two codes differ somewhat, particularly in the SOL, due to the manner in which the profiles are input to the two codes. Additionally, the full wave simulation represents a spectrum of n_{θ} with a single value of n_{ϕ} , while the ray tracing launches a spectrum of n_{\parallel} with $n_{\perp} \cdot \hat{\theta} = 0$. Here, n_{θ} , n_{ϕ} , and n_{\perp} are the poloidal, toroidal, and perpendicular indexes of refraction, and $\hat{\theta}$ is the poloidal unit vector. At this point, it is difficult to identify what physics may contribute to the differences between the two codes, especially if the difference is due to the limited validity of eikonal approximation used in ray tracing. A detailed comparison of the two codes to determine the cause of any substantive differences between ray tracing and full wave techniques is in progress and will be presented in a future publication.

Both the full wave and ray tracing simulations predict that LH wave absorption moves to

smaller minor radius as temperature, and thus single pass absorption, is increased. The large + symbol in Figure 9 indicates the predicted HXR emission from the GENRAY/CQL3D synthetic diagnostic for a discharge with $T_{e0} = 4$ keV. LHEAF/VERD predicts a similar enhancement of non-thermal emission as temperature increases (large asterisk symbol in Figure 9). Recent high density LHCD experiments on FTU also found increased non-thermal emission by raising the plasma temperature [36]. Fortunately the high bootstrap fraction scenarios which motivated the investigation of LHCD at high density are projected to have high temperature [14] and may show stronger absorption inside $r/a \sim 0.8$. Future burning plasma experiments will also have very high temperature and strong single pass damping, although large distances between the antenna and the LCFS may allow for substantial damping before the LH waves reach the confined plasma. Absorption between the antenna and the LCFS will be sensitive to the density and temperature profiles of the SOL, which are both very uncertain at this time.

Acknowledgments

The authors would like to thank the C-Mod LHCD engineering team for their efforts in keeping the system running. This work was supported by US Department of Energy awards DE-FC02-99ER54512 and DE-AC02-09CH11466.

-
- [1] P. T. Bonoli, R. Parker, S. J. Wukitch, Y. Lin, M. Porkolab, J. C. Wright, E. Edlund, T. Graves, L. Lin, J. Liptac, A. Parisot, A. E. Schmidt, V. Tang, W. Beck, R. Childs, M. Grimes, D. Gwinn, D. Johnson, J. Irby, A. Kanojia, P. Koert, S. Marazita, E. Mar-mar, D. Terry, R. Vieira, G. Wallace, J. Zaks, S. Bernabei, C. Brunkhorse, R. Ellis, E. Fredd, N. Greenough, J. Hosea, C. C. Kung, G. D. Loesser, J. Rushinski, G. Schilling, C. K. Phillips, J. R. Wilson, R. W. Harvey, C. L. Fiore, R. Granetz, M. Greenwald, A. E. Hubbard, I. H. Hutchinson, B. LaBombard, B. Lipschultz, J. Rice, J. A. Snipes, J. Terry, S. M. Wolfe, and the Alcator C-Mod Team, *Fusion Science and Technology*, **51**, 401 (2007).
- [2] I. H. Hutchinson, R. Boivin, F. Bombarda, P. Bonoli, S. Fairfax, C. Fiore, J. Goetz, S. Golovato, R. Granetz, M. Greenwald, S. Horne, A. Hubbard, J. Irby, B. LaBombard, B. Lipschultz,

- E. Marmor, G. McCracken, M. Porkolab, J. Rice, J. Snipes, Y. Takase, J. Terry, S. Wolfe, C. Christensen, D. Garnier, M. Graf, T. Hsu, T. Luke, M. May, A. Niemczewski, G. Tinios, J. Schachter, and J. Urbahn, *Physics of Plasmas*, **1**, 1511 (1994).
- [3] P. Bonoli, R. Parker, M. Porkolab, J. Ramos, S. Wukitch, Y. Takase, S. Bernabei, J. Hosea, G. Schilling, and J. Wilson, *Nuclear Fusion*, **40**, 1251 (2000).
- [4] R. Aymar, P. Barabaschi, and Y. Shimomura, *Plasma Physics and Controlled Fusion*, **44**, 519 (2002).
- [5] G. Wallace, A. Hubbard, P. Bonoli, I. Faust, R. Harvey, J. Hughes, B. LaBombard, O. Meneghini, R. Parker, A. Schmidt, S. Shiraiwa, A. Smirnov, D. Whyte, J. Wilson, J. Wright, S. Wukitch, and the Alcator C-Mod Team, *Nuclear Fusion*, **51**, 083032 (2011).
- [6] G. M. Wallace, R. R. Parker, P. T. Bonoli, A. E. Hubbard, J. W. Hughes, B. L. LaBombard, O. Meneghini, A. E. Schmidt, S. Shiraiwa, D. G. Whyte, J. C. Wright, S. J. Wukitch, R. W. Harvey, A. P. Smirnov, and J. R. Wilson, *Physics of Plasmas*, **17**, 082508 (2010).
- [7] N. J. Fisch and A. H. Boozer, *Physical Review Letters*, **45**, 720 (1980).
- [8] N. J. Fisch, *Reviews of Modern Physics*, **59**, 175 (1987).
- [9] R. R. Parker, S. Baek, O. Meneghini, C. Lau, Y. Podpaly, M. Porkolab, J. E. Rice, A. E. Schmidt, S. Shiraiwa, G. M. Wallace, S. J. Wukitch, and J. R. Wilson, *Bull. Am. Phys. Soc.*, **55**, 316 (2010).
- [10] S. Shiraiwa, O. Meneghini, R. Parker, G. Wallace, J. Wilson, I. Faust, C. Lau, R. Mumgaard, S. Scott, S. Wukitch, W. Beck, J. Doody, J. Irby, P. MacGibbon, D. Johnson, A. Kanojia, P. Koert, D. Terry, R. Vieira, and the Alcator C-Mod team, *Nuclear Fusion*, **51**, 103024 (2011).
- [11] O. Meneghini, S. Shiraiwa, W. Beck, J. Irby, P. Koert, R. R. Parker, R. Viera, J. Wilson, and S. Wukitch, *AIP Conference Proceedings*, **1187**, 423 (2009).
- [12] S. F. Knowlton and M. Porkolab, *Nuclear Fusion*, **29**, 1544 (1989).
- [13] R. Hawryluk, in *Physics of Plasmas Close to Thermonuclear Conditions, Volume 1*, edited by B. Coppi, G. G. Leotta, D. Pfirsch, R. Pozzoli, & E. Sindoni (1981) p. 19.
- [14] S. Shiraiwa, P. Bonoli, I. Faust, O. Meneghini, A. Hubbard, R. Parker, G. Wallace, and J. Wilson, *Bull. Am. Phys. Soc.*, **56**, 338 (2011).
- [15] D. Ignat, E. Valeo, and S. Jardin, *Nuclear Fusion*, **34**, 837 (1994).
- [16] V. E. Golant, *Soviet Physics Technical Physics*, **16**, 1980 (1972).

- [17] F. Troyon and F. W. Perkins, in *Proceedings of the 2nd Topical Conference on RF Plasma Heating*, edited by R. Dollinger, M. Kristiansen, M. O. Hagler, F. J. Paoloni, and J. Bergstroem (Texas Tech. Univ., Lubbock, TX, 1974) pp. B4.1–B4.6.
- [18] W. Hooke, *Plasma Physics and Controlled Fusion*, **26**, 133 (1984).
- [19] Y. Takase, M. Porkolab, J. J. Schuss, R. L. Watterson, C. L. Fiore, R. E. Slusher, and C. M. Surko, *Physics of Fluids*, **28**, 983 (1985).
- [20] M. Porkolab, *Physics of Fluids*, **20**, 2058 (1977).
- [21] M. Porkolab, S. Bernabei, W. M. Hooke, R. W. Motley, and T. Nagashima, *Physical Review Letters*, **38**, 230 (1977).
- [22] J. Liptac, R. Parker, V. Tang, Y. Peysson, and J. Decker, *Review of Scientific Instruments*, **77**, 103504 (2006).
- [23] R. W. Harvey and M. McCoy, in *Proceedings of the IAEA Technical Committee Meeting on Simulation and Modeling of Thermonuclear Plasmas* (1992) pp. 489–526.
- [24] A. P. Smirnov and R. Harvey, *Bull. Am. Phys. Soc.*, **40**, 1837 (1995).
- [25] M. Porkolab, J. J. Schuss, B. Lloyd, Y. Takase, S. Texter, P. Bonoli, C. Fiore, R. Gandy, D. Gwinn, B. Lipschultz, E. Marmor, D. Pappas, R. Parker, and P. Pribyl, *Physical Review Letters*, **53**, 450 (1984).
- [26] S. Knowlton, M. Porkolab, and Y. Takase, *Nuclear Fusion*, **28**, 99 (1988).
- [27] C. Lau, G. Hanson, J. Wilgen, Y. Lin, and S. Wukitch, *Review of Scientific Instruments*, **81**, 10D918 (2010).
- [28] R. M. McDermott, B. Lipschultz, J. W. Hughes, P. J. Catto, A. E. Hubbard, I. H. Hutchinson, R. S. Granetz, M. Greenwald, B. LaBombard, K. Marr, M. L. Reinke, J. E. Rice, and D. Whyte, *Physics of Plasmas*, **16**, 056103 (2009).
- [29] D. Whyte, A. Hubbard, J. Hughes, B. Lipschultz, J. Rice, E. Marmor, M. Greenwald, I. Cziegler, A. Dominguez, T. Golfopoulos, N. Howard, L. Lin, R. McDermott, M. Porkolab, M. Reinke, J. Terry, N. Tsujii, S. Wolfe, S. Wukitch, Y. Lin, and the Alcator C-Mod Team, *Nuclear Fusion*, **50**, 105005 (2010).
- [30] A. E. Hubbard, D. G. Whyte, R. M. Churchill, I. Cziegler, A. Dominguez, T. Golfopoulos, J. W. Hughes, J. E. Rice, I. Bespamyatnov, M. J. Greenwald, N. Howard, B. Lipschultz, E. S. Marmor, M. L. Reinke, W. L. Rowan, and J. L. T. A. C.-M. Group (Alcator C-Mod Group), *Physics of Plasmas*, **18**, 056115 (2011).

- [31] P. T. Bonoli and R. C. Englade, *Physics of Fluids*, **29**, 2937 (1986).
- [32] O. Meneghini, S. Shiraiwa, and R. Parker, *Physics of Plasmas*, **16**, 090701 (2009).
- [33] O. Meneghini, S. Shiraiwa, I. Faust, R. Parker, and G. Wallace, in *Proceedings of the 38th European Physical Society Conference on Plasma Physics*, edited by A. Becoulet (2011).
- [34] S. Shiraiwa, J. Ko, O. Meneghini, R. Parker, A. E. Schmidt, S. Scott, M. Greenwald, A. E. Hubbard, J. Hughes, Y. Ma, Y. Podpaly, J. E. Rice, G. Wallace, J. R. Wilson, S. M. Wolfe, and A. C.-M. Group, *Physics of Plasmas*, **18**, 080705 (2011).
- [35] O. Meneghini, *Fullwave modeling of lower hybrid waves on Alcator C-Mod*, Ph.D. thesis, Massachusetts Institute of Technology (2011).
- [36] R. Cesario, L. Amicucci, A. Cardinali, C. Castaldo, M. Marinucci, L. Panaccione, F. Santini, O. Tudisco, M. Apicella, G. Calabr, C. Cianfarani, D. Frigione, A. Galli, G. Mazzitelli, C. Mazzotta, V. Pericoli, G. Schettini, and A. Tuccillo, *Nat. Commun.*, **1**, 55 (2010).